Available online at www.sciencedirect.com
SCIENCE DIRECT®
Journal of Solid State Chemistry 177 (2004) 159–164
JOURNAL OF SOLID STATE CHEMISTRY
http://elsevier.com/locate/jssc

Non-centrosymmetric $Ba_3Ti_3O_6(BO_3)_2$

Hyunsoo Park, Anthony Bakhtiiarov, Wei Zhang, Ignacio Vargas-Baca, and Jacques Barbier*

Department of Chemistry, McMaster University, 1280 Main Street West, Hamilton, Ont., Canada L8S 4M1

Received 17 April 2003; received in revised form 16 June 2003; accepted 3 July 2003

Abstract

The compound previously reported as $Ba_2Ti_2B_2O_9$ has been reformulated as $Ba_3Ti_3B_2O_{12}$, or $Ba_3Ti_3O_6(BO_3)_2$, a new barium titanium oxoborate. Small single crystals have been recovered from a melt with a composition of $BaTiO_3$:$BaTiB_2O_6$ (molar ratio) cooled between 1100°C and 850°C. The crystal structure has been determined by X-ray diffraction: hexagonal system, non-centrosymmetric $P\bar{6}2m$ space group, $a = 8.7377(11)$ Å, $c = 3.9147(8)$ Å, $Z = 1$, $wR(F^2) = 0.039$ for 504 unique reflections. $Ba_3Ti_3O_6(BO_3)_2$ is isostructural with $K_3Ta_3O_6(BO_3)_2$. Preliminary measurements of nonlinear optical properties on microcrystalline samples show that the second harmonic generation efficiency of $Ba_3Ti_3O_6(BO_3)_2$ is equal to 95% of that of $LiNbO_3$.

Keywords: $Ba_3Ti_3O_6(BO_3)_2$; $Ba_3Ti_3B_2O_{12}$; Crystal structure; NLO properties

1. Introduction

The discovery, synthesis and crystal chemistry of new inorganic borates with potentially useful optical properties is of continuing interest [1–5]. Recent investigations by our group of ternary systems of the type MO–M'_2O_3–B_2O_3 (M = Sr, Ba, Pb; M' = Al, Ga, Fe, Mn) have led to the discovery of two new borate structure types including $MGa_2B_2O_7$ [6] and $PbM'BO_4$ [7,8]. These compounds are centrosymmetric and have no second-order nonlinear optical (NLO) properties but some of them, such as $PbMnBO_4$, display unusual one-dimensional magnetic properties [9]. In this work, attention is focussed on the BaO–TiO_2–B_2O_3 system in which previous studies have identified two ternary compounds: dolomite-type $BaTiB_2O_6$ [10,11] and a compound reported as $Ba_2Ti_2B_2O_9$ that could not be synthesized in pure form [12]. A search of the ICDD database [13] revealed that the hexagonal unit-cell determined for $Ba_2Ti_2B_2O_9$ ($a = 8.721$ Å, $c = 3.933$ Å) was in fact very similar to the unit-cells of the non-centrosymmetric borates, $K_3Ta_3O_6(BO_3)_2$ ($a = 8.781$ Å, $c = 3.899$ Å) [14,15] and the high-temperature form of $K_3Nb_3O_6(BO_3)_2$ ($a = 8.779$ Å, $c = 3.983$ Å) [16]. This observation suggested that "$Ba_2Ti_2B_2O_9$" should be re-formulated as $Ba_3Ti_3B_2O_{12}$, or more precisely $Ba_3Ti_3O_6(BO_3)_2$. Our results confirm the correct composition of this new barium titanium oxoborate and contradict a very recent survey of the BaO–TiO_2–B_2O_3 system [35] in which the incorrect "$Ba_2Ti_2B_2O_9$" composition was again reported. The synthesis and structure determination of $Ba_3Ti_3O_6(BO_3)_2$ are presented here together with the preliminary measurements of its NLO properties.

2. Solid-state synthesis and crystal growth

Polycrystalline samples of $Ba_3Ti_3O_6(BO_3)_2$ were synthesized by solid-state reactions of stoichiometric amounts of $BaCO_3$ (99%, J.T. Baker) or $Ba(NO_3)_2$ (99%, Alfa Aesar), TiO_2 (99.9%, Cerac) and $B(OH)_3$ (99.99%, Alfa Aesar). After dehydration of boric acid by slow heating to 500°C, 0.5 g pellets were heated up to 900°C for several days with several intermediate re-mixings. The reaction products were analyzed by powder X-ray diffraction (Guinier-Hägg camera, Cu$K\alpha_1$ radiation, Si internal standard). In all syntheses, a minor or trace amount of $BaTiO_3$ perovskite was identified in the products, even after prolonged heating of a sample for 10 days at 900°C. This was likely the result of a slight loss of B_2O_3 by evaporation at high temperature since

*Corresponding author. Fax: +905-522-2509.
E-mail address: barbier@mcmaster.ca (J. Barbier).

0022-4596/$ - see front matter © 2003 Elsevier Inc. All rights reserved.
doi:10.1016/S0022-4596(03)00389-X

addition of a small excess of $B(OH)_3$ (10 mol%) to the starting mixture eliminated $BaTiO_3$ from the products and led to the formation of some $BaTiB_2O_6$ instead. The synthesis was also carried out using starting mixtures containing either stoichiometric amounts of $BaTiO_3$ perovskite (99.99%, Aldrich) and $B(OH)_3$, or stoichiometric amounts of $BaTiO_3$ and pre-reacted $BaTiB_2O_6$. A trace amount of perovskite was present in the products of these reactions as well. Overall, it was observed that either $BaTiO_3$ or $BaTiB_2O_6$ formed more readily than $Ba_3Ti_3O_6(BO_3)_2$ which only appeared in the products of solid-state reactions for temperatures above 800°C. This observation is in agreement with the results of our crystal growth experiments in which crystals of $BaTiO_3$ and $BaTiB_2O_6$ were more readily obtained than crystals of $Ba_3Ti_3O_6(BO_3)_2$. The possibility that $Ba_3Ti_3O_6(BO_3)_2$ is thermodynamically stable at high temperature only has not been further investigated in this work.

As noted by previous authors for the hypothetical $Ba_2Ti_2B_2O_9$ compound [12], $Ba_3Ti_3O_6(BO_3)_2$ was found to melt incongruently at temperatures above 950°C. Therefore, crystallization experiments were carried out by slowly cooling melts of various compositions intermediate between $BaTiO_3$ and $BaTiB_2O_6$, and the best results were obtained by using a 1:1 mixture (molar ratio). A 12 g sample was melted at 1100°C in a covered platinum crucible, held at that temperature for 3 h, cooled to 850°C at 1°C h^{-1} and quenched in air. The crystallization products consisted of colorless hexagonal plates of $BaTiB_2O_6$ as the major phase, together with light yellow blocky crystals of tetragonal $BaTiO_3$ and light green-yellow prisms of $BaTi_2O_5$, plus small colorless hexagonal plates of $Ba_3Ti_3O_6(BO_3)_2$. Because the latter were difficult to distinguish from the $BaTiB_2O_6$ plates under the optical microscope, suitable single crystals of $Ba_3Ti_3O_6(BO_3)_2$ were identified by determining their unit-cell parameters with a single-crystal diffractometer.

Unsuccessful attempts were made to extend the crystal chemistry of the $Ba_3Ti_3O_6(BO_3)_2$ structure-type via substitution of the Ba^{2+} and/or Ti^{4+} cations, as suggested by the isostructural relationship with $K_3M_3B_2O_{12}$ (M = Ta, Nb) [14–16]. For example, although dolomite-type $BaSnB_2O_6$ exists [1] and can be readily synthesized by solid-state reactions, $Ba_3Sn_3B_2O_{12}$ could not be synthesized in our experiments, which yielded a mixture of $BaSnO_3$ and $BaSnB_2O_6$ instead. Similarly, only perovskite-type phases were recovered in the attempted syntheses of $Pb_3Ti_3B_2O_{12}$, $Pb_3Sn_3B_2O_{12}$ and $Sr_3Ti_3B_2O_{12}$. Finally, the formation of a solid solution between the isostructural $Ba_3Ti_3O_6(BO_3)_2$ and $K_3Ta_3O_6(BO_3)_2$ compounds was investigated by solid-state reactions of either unreacted starting materials or pre-reacted end-members. Surprisingly, only very limited solid solution (5–10% at most) was found to form at either end of the $Ba_3Ti_3O_6(BO_3)_2$–$K_3Ta_3O_6(BO_3)_2$ system. Complex oxide compounds formed instead with, for instance, a compound closely related to $Ba_3Ti_4Ta_4O_{21}$ [17] forming as the major phase in a 1:1 mixture of pre-reacted end-members heated up to 900°C for several days.

3. Structure determination

The structure of $Ba_3Ti_3O_6(BO_3)_2$ was determined by single-crystal X-ray diffraction using intensity data collected on a Bruker P4 diffractometer equipped with a Mo$K\alpha$ rotating anode X-ray source and a SMART 1K CCD area detector. The raw intensity data were first corrected for Lorentz and polarization effects with the computer software SAINT [18] and an empirical absorption correction was then applied using the program SADABS [19]. The details of the crystal data and the refinement procedure are given in Table 1. The structure solution was obtained in the non-centrosymmetric hexagonal space group $P\bar{6}2m$ with the programs SHELXS [20] and SHELXL97 [21]. The lack of a center of symmetry was confirmed by observing a second harmonic generation (SHG) signal using a polycrystalline sample (initial test performed by A. Kahn-Harari at École Nationale Supérieure de Chimie de Paris, France—see also below). The full least-squares refinement of 27 parameters was then carried out with anisotropic displacement parameters for all atoms, a secondary extinction parameter and a chiral twin parameter (refined to 0.04(4) indicating that the crystal

Table 1
Crystallographic data and refinement details for $Ba_3Ti_3O_6(BO_3)_2$

Crystal system	Hexagonal
Space group	$P\bar{6}2m$
Unit-cell parameters (Å)	$a = 8.7377(11)$
	$c = 3.9417(8)$
Unit-cell volume (Å^3)	260.62
Z	1
Calc. density (g cm^{-3})	4.902
Wavelength	Mo$K\alpha$
Crystal dimensions (mm)	$0.15 \times 0.20 \times 0.30$
Absorption coefficient (mm^{-1})	13.40
2θ max (deg)	72.61
Index ranges	$-13 < h < 14$
	$-14 < k < 11$
	$-5 < l < 6$
Unique reflections	504
Absorption correction	SADABS
T_{min}/T_{max}	0.599
BASF (chiral twinning parameter)	0.04(4)
R_{int}	0.036
Refined parameters	27
Goodness-of-fit	1.208
$R[F > 4\sigma(F)]$	0.016 (for 493 reflections)
w$R(F^2)$	0.039
Difference map (e Å^{-3})	1.04 (1.38 Å from Ba)
	−1.00 (0.74 Å from Ba)

Table 2
Atomic coordinates and equivalent isotropic displacement parameters for $Ba_3Ti_3O_6(BO_3)_2$

Atom	x	y	z	U_{eq}(Å^2)
Ba	0	0.60021(4)	1/2	0.00860(9)
Ti	0	0.23664(11)	0	0.0087(2)
B	2/3	1/3	0	0.0057(10)
O_1	0	0.2606(6)	1/2	0.0168(9)
O_2	0	0.8103(4)	0	0.0076(6)
O_3	0.6778(5)	0.4942(5)	0	0.0197(7)

(a) Anisotropic displacement parameters for $Ba_3Ti_3O_6(BO_3)_2$

	U_{11}	U_{22}	U_{33}	U_{23}	U_{13}	U_{12}
Ba	0.0099(2)	0.0086(1)	0.0078(1)	0	0	0.00497(7)
Ti	0.0030(4)	0.0036(3)	0.0193(4)	0	0	0.0015(2)
B	0.004(2)	0.004(2)	0.009(2)	0	0	0.0021(8)
O_1	0.017(2)	0.014(1)	0.020(2)	0	0	0.008(1)
O_2	0.005(2)	0.005(1)	0.013(1)	0	0	0.0023(8)
O_3	0.014(2)	0.008(1)	0.039(2)	0	0	0.007(1)

Table 3
Bond distances (l), bond valences (s) and bond valence sums ($\sum s$) in $Ba_3Ti_3O_6(BO_3)_2$

	l (Å)	s (observed)[a]	s (predicted)[b]
Ba–O1	2.968(5)	0.160	0.185
Ba–O1 × 2	3.071(1)	0.121	0.185
Ba–O2 × 2	2.693(3)	0.336	0.203
Ba–O3 × 4	2.909(3)	0.188	0.130
Ba–O3 × 4	3.172(3)[c]	0.092	0.130
$\sum s$		**2.19**	**2.00**
Ti–O1 × 2	1.9819(7)	0.637	0.722
Ti–O2 × 2	1.896(1)	0.803	0.797
Ti–O3 × 2	2.081(3)	0.487	0.481
$\sum s$		**3.85**	**4.00**
B–O3 × 3	1.360(3)	1.030	1.000
$\sum s$		**3.09**	**3.00**
O1–Ba	2.968(5)	0.160	0.185
Ba × 2	3.071(1)	0.121	0.185
Ti × 2	1.9819(7)	0.637	0.722
$\sum s$		**1.68**	**2.00**
O2–Ba × 2	2.693(3)	0.336	0.203
Ti × 2	1.896(1)	0.803	0.797
$\sum s$		**2.28**	**2.00**
O3–Ba × 2	3.172(3)	0.092	0.130
Ba × 2	2.909(3)	0.188	0.130
Ti	2.081(3)	0.487	0.481
B	1.360(3)	1.030	1.000
$\sum s$		**2.08**	**2.00**

[a] Calculated using the equation $s_i = \exp[(r_0 - r_i)/0.37]$ introduced by Altermatt and Brown [27] and the r_0 bond valence parameters of Brese and O'Keeffe [34].

[b] Predicted using the method described by O'Keeffe [28,29].

[c] The next Ba–O distance is 4.479 Å with a negligible bond valence of 0.003 v.u.

used was essentially untwinned). The refinement converged to $wR(F^2) = 0.039$ for 504 unique reflections. The atomic positions and equivalent isotropic temperature parameters for $Ba_3Ti_3O_6(BO_3)_2$ are given in Table 2, and the anisotropic displacement parameters are listed in Table 2a. The bond distances and the corresponding bond valences and bond valence sums are listed in Table 3.

The anisotropy observed for the U parameters of the Ti and O3 atoms (Table 2a) led us to attempt the structure refinement in two subgroups of $P\bar{6}2m$, namely $P31m$ and $P\bar{6}$. These refinements, however, did not produce any significant improvement and furthermore indicated the presence of additional two-fold axes perpendicular to the c-axis in P31 m, or mirror planes parallel to the c-axis in $P-6$. It was therefore concluded that the $Ba_3Ti_3O_6(BO_3)_2$ structure is best described in the same $P\bar{6}2m$ space group symmetry as $K_3Ta_3O_6(BO_3)_2$ [15] and the high-temperature form of $K_3Nb_3O_6(BO_3)_2$ [16].

4. Description and bond valence analysis of the $Ba_3Ti_3O_6(BO_3)_2$ structure

The structure is illustrated in Fig. 1. It consists of trimers of corner-sharing TiO_6 octahedra which are interconnected by BO_3 groups to form (001) layers. These layers are linked in the c direction by the apical O_1 atoms of the TiO_6 octahedra to create a three-dimensional $Ti_3B_2O_{12}^{6-}$ framework with [001] triple octahedral chains. The Ba^{2+} cations are located in irregular pentagonal tunnels parallel to the c-axis and their coordination can be described as a tricapped pentagonal prism by including all the Ba–O bonds up to 3.17 Å (Table 3). Similar coordination environments occur in the isostructural borates $K_3M_3O_6(BO_3)_2$ (M = Ta, Nb) [14–16,22] and in the related silicates $Ba_{1.5}Nb_3O_6(Si_2O_7)$ and $K_3Nb_3O_6(Si_2O_7)$ [23–26].

The bond valence analysis of the $Ba_3Ti_3O_6(BO_3)_2$ structure yields adequate bond valence sums with only

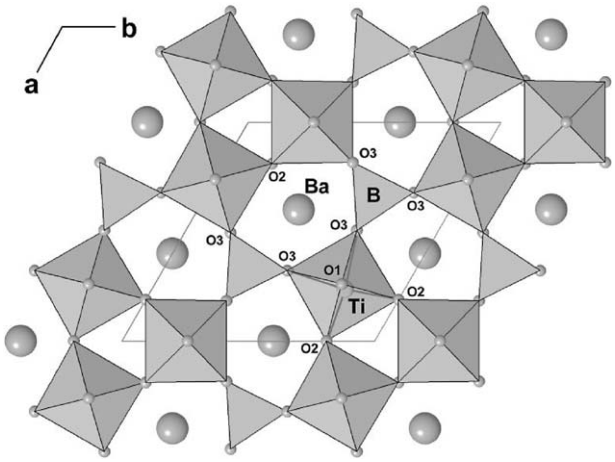

Fig. 1. View of the $Ba_3Ti_3O_6(BO_3)_2$ structure projected on the (001) plane of the hexagonal unit cell. The off-center displacement of the Ti^{4+} cations has been illustrated for one of the TiO_6 octahedra.

minor deviations from their expected values except for the O_1 and O_2 atoms which are significantly underbonded ($\sum s = 1.68$) and overbonded ($\sum s = 2.28$), respectively (Table 3). The bond valences expected from the bond topology of the $Ba_3Ti_3O_6(BO_3)_2$ structure have also been calculated using the method described by O'Keeffe [28,29]. In this method, the valences of individual bonds are predicted by solving a system of equations expressing the bond valence sum rule at the "cation" and "anion" sites and the connectivity, or bond topology, within a crystal structure. For the $Ba_3Ti_3O_6(BO_3)_2$ structure, the comparison of the observed and predicted bond valences (Table 3) leads to the following conclusions:

(i) The distortion of the TiO_6 octahedra is mostly a result of the bond topology as shown by the correct prediction of different bond valences for the Ti–O bonds, increasing in the order Ti–O3 < Ti–O1 < Ti–O2 with a wide spread of valences from 0.48 to 0.80 valence units (v.u.) (Table 3). In particular, the large difference between the short Ti–O2 and long Ti–O3 bonds (associated with the 0.2 Å off-center shift of the Ti^{4+} cations in the TiO_6 octahedra—Fig. 1) is well predicted by the bond valence analysis. Similar octahedral distortions are present in $K_3Ta_3O_6(BO_3)_2$ [6] and $K_3Nb_3O_6(BO_3)_2$ [7] and can also be attributed to the bond topology of that particular structure type. The slight underbonding of the Ti site arises from the stretching of the Ti–O1 bonds ($s_{observed} = 0.64$ v.u. vs. $s_{predicted} = 0.72$ v.u.) which must be due to non-bonded interactions, such as $Ba^{2+} \cdots Ti^{4+}$ repulsions.

(ii) The underbonding of the O1 position is due to the systematic stretching of the Ti–O1 and Ba–O1 bonds (with smaller bond valences than predicted), whereas the overbonding of the O2 atom is due mainly to the compression of the Ba–O2 bonds (with a larger bond valence than predicted) (Table 3). The $Ba_3Ti_3O_6(BO_3)_2$ structure contains, therefore, both tensile and compressive residual bond strain which cannot be easily relieved: as seen in Fig. 1, the Ba–O1 bonds cannot be shortened without also shortening the already compressed Ba–O2 bonds. The bond strain can be quantified by calculating the index $R = \langle (V_i - \sum s_{ij})^2 \rangle^{1/2}$ equal to the root-mean square of the bond-valence sum deviations, with V_i and $\sum s_{ij}$ representing the oxidation state and the bond valence sum of atom i, respectively [30]. For $Ba_3Ti_3O_6(BO_3)_2$, $R = 0.19$ v.u. (with major contributions from the bond valence sums around the O1 and O2 atoms—Table 3), close to the limiting value of 0.2 v.u. which has been proposed as an indicator of instability of a crystal structure and of the possible occurrence of phase transitions [30,31]. Apart from the slight anisotropy in some of the atomic displacement parameters mentioned above, no indication of a phase transition of the type reported in $K_3Nb_3O_6(BO_3)_2$ [16,22] has been observed in the present study of $Ba_3Ti_3O_6(BO_3)_2$. Nevertheless, the presence of bond strain in its crystal structure may well play a role in its apparent marginal stability by comparison with $BaTiO_3$ and $BaTiB_2O_6$.

5. Measurement of nonlinear optical (NLO) properties

The efficiency of SHG in $Ba_3Ti_3O_6(BO_3)_2$ (BTBO) was evaluated by the Kurtz–Perry method [32] using a microcrystalline sample synthesized by solid-state reaction and containing a trace amount of $BaTiO_3$ perovskite. About 50 mg of sieved powder (particle size in the 53–75 μm range) was hand-pressed into a 7 mm-diameter pellet which was irradiated with a pulsed infrared beam (5 ns, 10 mJ, 10 Hz) produced by an optical parametric oscillator pumped by a Nd:YAG laser. A dichroic mirror was used to separate the signal (measured in the reflection mode) from the fundamental and stir the visible light onto a photomultiplier. A combination of a half-wave achromatic retarder and a polarizer was used to control the intensity of the incident power (P_ω), which was measured with a fast IR photodiode. The intensity of the second harmonic signal ($P_{2\omega}$) was fitted to

$$P_{2\omega} = K d_{\text{eff}}^2 P_\omega^2.$$

All the measurements were referred to a sample of $LiNbO_3$ (LNbO) powder (certified reagent from Fisher Scientific, sieved to the same particle size as the BTBO sample). The K factor was taken to be constant

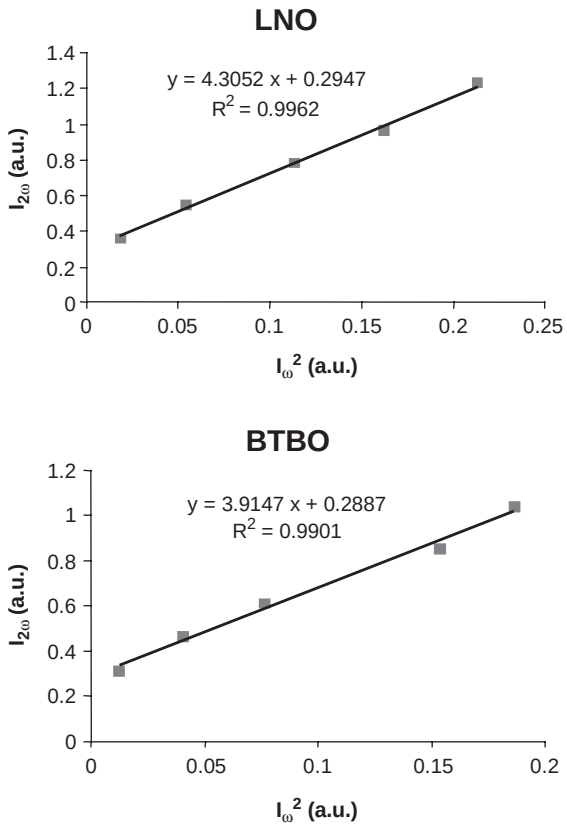

Fig. 2. Mesurement of the powder SHG efficiencies of $LiNbO_3$ (LNO, top) and $Ba_3Ti_3O_6(BO_3)_2$ (BTBO, bottom) at a fundamental wavelength (ω) of 1064 nm.

assuming that the BTBO and LNbO samples have similar refractive indices. The absolute SHG efficiency of BTBO was nearly constant within the range of fundamental wavelengths investigated (900–1400 nm). At the wavelength of 1064 nm, the relative efficiency $d_{\mathrm{eff}}(\mathrm{BTBO})/d_{\mathrm{eff}}(\mathrm{LNbO})$ was determined to be equal to 0.95 ± 0.01 (Fig. 2). This value compares very favorably with the relative efficiencies quoted for other NLO borates, such as LiB_3O_5 (LBO, $d_{\mathrm{eff}} = 0.17 \times d_{\mathrm{eff}}(\mathrm{LNbO})$) or BaB_2O_4 (BBO, $d_{\mathrm{eff}} = 0.33 \times d_{\mathrm{eff}}(\mathrm{LNbO})$) [33].

The large SHG efficiency of BTBO is in agreement with the conclusions of a recent review of NLO properties of inorganic borates [1] where it was found that a common orientation of the anionic BO_3^{3-} groups parallel the polar axis of a non-centrosymmetric crystal structure is favorable for the obtention of large SHG coefficients. This is indeed the case in $Ba_3Ti_3O_6(BO_3)_2$ where all the BO_3 groups have a strictly planar, regular triangular geometry and are parallel to the $\langle 100 \rangle$ and $\langle 110 \rangle$ polar two-fold axes of the structure with only a small misorientation of 3.1° between two adjacent BO_3 groups (Fig. 1). However, apart from the borate groups, the asymmetrical Ti–O bonds in the TiO_6 octahedra (associated with a 0.2 Å off-center displacement of the Ti^{4+} cations) are also expected to contribute significantly to the overall SHG efficiency of BTBO.

$Ba_3Ti_3O_6(BO_3)_2$ is the first example of a titanium oxoborate with potentially useful NLO properties. Further work is now in progress to improve its synthesis and to investigate the growth of larger single crystals.

Acknowledgments

This work was supported by research grants from the Canadian Natural Sciences and Engineering Research Council to JB and IVB, grants from the Canadian Foundation for Innovation and the Ontario Innovation Trust to IVB, and an Ontario Graduate Scholarship to HP. The single-crystal data were collected by Dr. J. Britten in the Department of Chemistry at McMaster University. An initial measurement of NLO properties by A. Kahn-Harari at the École Nationale Supérieure de Chimie de Paris is gratefully acknowledged.

References

[1] P. Becker, Adv. Mater 10 (1998) 979–992.
[2] T. Sasaki, Y. Mori, M. Yoshimura, Y.K. Yap, T. Kamimura, Mater. Sci. Eng. R 30 (2000) 1–54.
[3] P. Becker, Z. Kristallogr. 216 (2001) 523–533.
[4] M.J. Barber, P. Becker, Z. Kristallogr. 217 (2002) 205–211.
[5] E. Parthé, Z. Kristallogr. 217 (2002) 179–200.
[6] H. Park, J. Barbier, J. Solid State Chem. 154 (2000) 598–602.
[7] H. Park, J. Barbier, Acta Crystallogr. E 57 (2001) 82–84.
[8] H. Park, R.P. Hammond, J. Barbier, Solid State Sci. 5 (2003) 565–571.
[9] H. Park, R. Lam, J.E. Greedan, J. Barbier, Chem. Mater. 15 (2003) 1703–1712.
[10] J. Vicat, S. Aléonard, Mater. Res. Bull. 3 (1968) 611–620.
[11] G. Bayer, Z. Kristallogr. 133 (1971) 85–90.
[12] J.M. Millet, R.S. Roth, H.S. Parker, J. Am. Ceram. Soc. 69 (1986) 811–814.
[13] PCPDFWIN database, Joint Committee on Powder Diffraction Standards-International Center for Diffraction Data, 2002.
[14] J. Choisnet, D. Groult, B. Raveau, M. Gasperin, Acta Crystallogr. B 33 (1977) 1841–1845.
[15] S.C. Abrahams, L.E. Zyontz, J.L. Bernstein, J.P. Remeika, A.S. Cooper, J. Chem. Phys. 75 (1981) 5456–5460.
[16] P. Becker, L. Bohaty, J. Schneider, Crystallogr. Rep. 42 (1997) 213–217.
[17] C. Mercey, D. Groult, B. Raveau, Rev. Chim. Miner. 16 (1979) 165–173.
[18] SAINT Version 6.02, Bruker AXS Inc., Madison, WI, USA, 2000.
[19] G.M. Sheldrick, Siemens Area Detector Absorption Correction Software, University of Göttingen, Germany, 2001.
[20] G.M. Sheldrick, Acta Crystallogr. A 46 (1990) 467–473.
[21] G.M. Sheldrick, SHELXL97 Program for the Refinement of Crystal Structures, University of Göttingen, Germany, 1997.
[22] P. Becker, P. Held, L. Bohaty, Z. Kristallogr. 211 (1996) 449–452.
[23] J. Shannon, L. Katz, Acta Crystallogr. B 26 (1970) 105–109.
[24] J. Choisnet, N. Nguyen, D. Groult, B. Raveau, Mater. Res. Bull. 11 (1976) 887–894.

[25] J. Choisnet, N. Nguyen, D. Groult, B. Raveau, Mater. Res. Bull. 12 (1977) 91–96.
[26] S. Jaulmes, S. Launay, P. Mahé, M. Quarton, Acta Crystallogr. C 51 (1995) 794–796.
[27] D. Altermatt, I.D. Brown, Acta Crystallogr. B 41 (1985) 240–244.
[28] M. O'Keeffe, Struct. Bonding (Berlin) 71 (1989) 162–190.
[29] M. O'Keeffe, Acta Crystallogr. A 46 (1990) 138–142.
[30] I.D. Brown, Acta Crystallogr. B 48 (1992) 553–572.
[31] T. Armbruster, F. Röthlisberger, F. Seifert, Am. Mineral. 75 (1990) 847–858.
[32] S.K. Kurtz, T.T. Perry, J. Appl. Phys. 39 (1968) 3798–3813.
[33] M.H. Dunn, M. Ebrahimzadeh, Science 286 (1999) 1513–1517.
[34] N.E. Brese, M. O'Keeffe, Acta Crystallogr. B 47 (1991) 192–197.
[35] S.Y. Zhang, M. He, X.L. Chen, X. Wu, Y.G. Gao, Y.T. Song, D.Q. Ni, Mater. Res. Bull. 38 (2003) 783–788.